**Proceedings of the ASME Symposium on Elevated Temperature Application of Materials for Fossil, Nuclear, and Petrochemical Industries**
**March 25-27, 2014**

**ETAM2014-1033**

# CONSTITUTIVE MODELING OF HAYNES 230 FOR HIGH TEMPERATURE FATIGUE-CREEP INTERACTIONS

**Paul R. Barrett, Raasheduddin Ahmed, Tasnim Hassan**
North Carolina State University
Raleigh, NC, USA

## ABSTRACT

Non-linear stress analysis for high temperature cyclic viscoplasticity is increasingly becoming an important modeling framework for many industries. Simplified analyses are found to be insufficient in accurately predicting the life of components; such as a gas turbine engine of an airplane or the intermediate-heat exchanger of a nuclear power plant. As a result, advanced material models for simulating nonlinear responses at room to high temperature are developed and experimentally validated against a broad set of low-cycle fatigue responses; such as creep, fatigue, and their interactions under uniaxial stress states. . This study will evaluate a unified viscoplastic model based on nonlinear kinematic hardening (Chaboche type) with several added features of strain-range-dependence, rate-dependence, temperature-dependence, static recovery, and mean-stress-evolution for Haynes 230database. Simulation-based model development for isothermal creep-fatigue responses are all critically evaluated for the developed model. The robustness of the constitutive model is demonstrated and weaknesses of the model to accurately predict low-cycle fatigue responses are identified.

**Keywords:** Constitutive modeling, Isothermal fatigue, Stress relaxation, Haynes 230, Creep-Fatigue, High temperature fatigue.

## NOMENCLATURE

| | |
|---|---|
| $C_i$ | Kinematic hardening parameter |
| $D_{\gamma i}$ | Kinematic hardening evolution rate parameter |
| $E$ | Young's modulus |
| $H$ | Heaviside function |
| **I** | Identity tensor |
| IP | In-phase |
| $J(\ )$ | Second invariant |
| $K$ | Rate dependent parameter |
| LCF | Low cycle fatigue |
| N | Number of cycles |
| OP | Out-of-phase |
| $T$ | Temperature |
| TMF | Thermo-mechanical fatigue |
| **Y** | Center of strain memory surface |
| $\mathbf{Y}_{\mathbf{bi}}$ | Second order tensor modifying back stress |
| $Y_{st,i}$ | Back stress modification variable evolution parameter |
| **a** | Deviator of back stress |
| $\mathbf{a}_i$ | Deviator of a back stress component |
| $a_{\gamma i}$ | Kinematic hardening evolution parameter |
| $b_i$ | Kinematic hardening static recovery parameter |
| $b_{\gamma i}$ | Kinematic hardening evolution parameter |
| $c_{\gamma i}$ | Kinematic hardening evolution parameter |
| $g$ | Strain memory surface |
| $m_{sr}$ | Strain memory surface radius evolution parameter |
| **n** | Normal to viscoplastic potential surface |
| **n*** | Normal to strain memory surface |
| p | Cumulative inelastic strain |
| $q$ | Radius of strain memory surface |
| $r_i$ | Kinematic hardening static recovery parameter |
| **s** | Deviatoric stress tensor |
| $t$ | Time |
| $tr$ | Trace of tensor |
| **α** | Back stress |
| $\alpha_b$ | Back stress modification variable evolution parameter |
| $\gamma_i$ | Kinematic hardening parameter |
| $\gamma_i^{AS}$ | Kinematic hardening evolution parameter |
| $\Delta\varepsilon$ | Strain range |
| **ε** | Strain tensor |
| $\boldsymbol{\varepsilon}^{\mathbf{e}}$ | Elastic strain tensor |
| $\boldsymbol{\varepsilon}^{\mathbf{in}}$ | Inelastic strain tensor |
| $\eta$ | Strain memory surface radius evolution parameter |
| $\nu$ | Poisson's ratio |
| $\xi$ | Strain memory surface radius evolution parameter |
| **σ** | Stress tensor |
| $\sigma_o$ | Yield stress |
| $(\bullet)$ | Differentiation with respect to time |
| A | Rate saturation parameter of sine hyperbolic flow rule |
| α | Rate saturation parameter of exponential flow rule |

## INTRODUCTION

Nickel-base superalloys have been favored in the high temperature service areas of components in the aerospace and nuclear power industries owing to their excellent mechanical properties at elevated temperatures. Over the past three decades, the characterization of these nickel-base superalloys under service-like testing conditions has been of great research interest. Service-conditions of nickel-base superalloy components in the aerospace and nuclear power industries experience start-up and shut-down cycles that induce repeated thermo-mechanical stresses. Under these high temperature thermo-mechanical cycles, damage accumulates eventually leading to a component failure. High temperature component failures are primarily induced by out-of-phase thermo-mechanical, creep-fatigue damage accumulation among many other factors [1-4]. Despite the use of high temperature resistant nickel-base superalloys, premature cracking in a component occurs which significantly increases the operation and maintenance expenses. Material responses of these critical components may involve time-dependent processes such as creep, oxidation, dynamic strain aging, creep-fatigue, thermo-mechanical fatigue and cyclic creep or ratcheting that influence the integrity of the component [5].

It is necessary to understand these complex material responses, under realistic loading conditions to improve current design methodologies. Current industry standards uses life prediction methods based on either simple elastic analyses or simplified inelastic models using commercial finite element analysis (FEA) software, which lack fidelity in simulating the low-cycle fatigue responses. An accurate description of thermo-mechanical cyclic stress-strain responses during service is essential for the development of reliable life prediction techniques for critical components in elevated temperature applications. This requires the development of an appropriate robust constitutive model capable of describing the interaction of different time and temperature-dependent phenomena which occur as a result of very high temperature operation.

The study reported herein performed a broad set of uniaxial creep-fatigue experiments on Haynes 230 at room to elevated temperatures, thereby creating similar conditions that the combustor liner of a gas-turbine engine experiences. These experiments were conducted prescribing different isothermal loading histories from 24°C to 982°C with different strain rates and strain ranges. The effect of strain hold times known as creep-fatigue interaction was also investigated by prescribing different hold times. The hold durations of these strain-controlled creep-fatigue tests were of 1 and 2 minutes due to time-constraint and economy. As a result, fatigue-creep was more appropriate as the predominant damage mechanism because of significantly more fatigue damage compared to the creep damage. In order to investigate further the creep responses of the material, pure creep tests were conducted, which are stress-controlled tests. This set of isothermal experimental results was important for model development progressively from simple phenomena to the more representative service conditions often seen in elevated temperature components, which is anisothermal thermo-mechanical fatigue. Anisothermal simulation of thermo-mechanical fatigue material responses requires model development at isothermal temperatures; such that, material parameters are known at incremental temperatures.

The unified viscoplastic constitutive model presented herein is of the Chaboche-type [6-8]. Due to the material complexity of Haynes 230 several features needed to be added in order to properly simulate both isothermal and anisothermal material responses. Cyclic hardening through the kinematic rule proposed by Krishna et al., 2009 [9] combined with the plastic strain memory surface theories for strain range dependence proposed by Chaboche et al., 1979 [10] was needed for Haynes 230. Haynes 230 isothermal cyclic stress evolution was both temperature and strain range dependent that was kinematic in nature rather than isotropic. Two main ingredients of cyclic viscoplasticity, rate-dependence and static recovery, were implemented based on Chaboche, 1989 [7]. However, due to the presence of a non-zero cyclic mean stress in the isothermal fatigue-creep experiments with strain dwells, the non-linear kinematic hardening rule was developed further for four backstresses incorporating the concepts presented by Yaguchi et al. and Ahmed et al. [11-12]. The experimental validation against the isothermal fatigue and fatigue-creep responses in the development of an advanced constitutive model is necessary before undertaking the thermo-mechanical fatigue responses. Finally, the modeling of rate saturation was explored for various flow rules and the modeling challenges of simulating both fatigue and creep responses is presented.

## EXPERIMENTAL STUDY

*Uniaxial Isothermal Experiments*

A large number of strain-controlled experiments were conducted in an effort to characterize the material behavior of Haynes 230 under fatigue-creep loading. These tests were uniaxial as the component of interest in the present study is the combustor liners of gas-turbine engines, which in service experience primarily uniaxial loading conditions. However finite element analysis has shown that some parts of the liner may experience multiaxial loading and for that reason a number of multiaxial tests were planned. This includes a total of 14 tension-torsion ratcheting and tension-torsion out-of-phase tests at various temperatures ranging from 24°C to 982°C which were presented in Ahmed et al., 2013 [12].

Isothermal low cycle fatigue tests with symmetric, axial strain controlled loading histories were performed at various strain rates and peak strain hold (dwell periods). The loading waveform was triangular for experiments without hold times, and trapezoidal for experiments with hold times. Three loading strain rates of 0.2 cycles per minute (cpm), 2 cpm and 20 cpm were prescribed in the experiments at temperatures ranging from 25°C to 982°C. The loading strain rates of 0.2, 2, and 20 cpm are in the order of $10^{-5}$ to $10^{-3}$ $s^{-1}$ respectively. The

imposed strain ranges varied from 0.3 to 1.6%. The types of loading histories for isothermal tests are presented in Figure 1. Figure 1a shows a typical axial strain-controlled LCF test that can be conducted at varying strain range, strain rate, and temperature to develop the constitutive model for strain range dependence, strain rate dependence, and temperature dependence. Figure 1b shows a fatigue-creep test with strain dwells at the compressive peak. In Fig. 1b, tests can be varied in addition to strain range, strain rate, and temperature for various strain dwell times (hold times). Figure 1b allows one to characterize the isothermal fatigue-creep interactions and the viscosity of the material needed for constitutive model development. The fatigue-creep tests of Fig. 1b were conducted at isothermal temperatures ranging from 649°C to 982°C (1200°F to 1800°F). Hold periods, $t_H$, of 60 and 120 seconds were imposed to investigate the effect of various hold times. Operating temperatures were in the range where creep deformation occurs, so that the interaction between LCF and creep can be investigated.

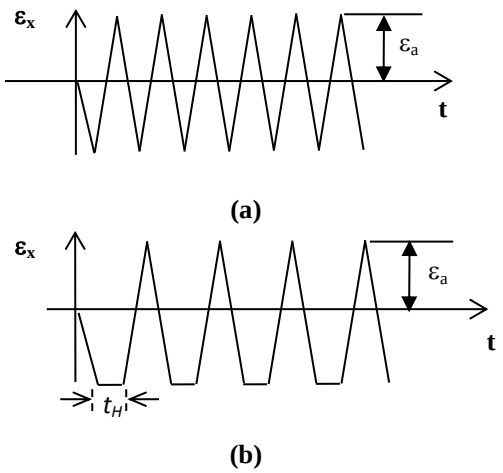


**Fig. 1:** Isothermal LCF, symmetric axial strain cycling (a) without holds, and (b) with strain holds

The investigation of creep was also done on Haynes 230 using traditional creep tests for stress-controlled loading histories at various creep stress levels. A typical stress-controlled loading for creep is shown in Fig. 2. The creep responses were used to validate the developed constitutive model against not only the fatigue-type damage, but also creep-type damage; thus, understanding the two extremes in the fatigue-creep interaction. Creep temperatures investigated were from 649°C to 982°C (1200°F to 1800°F).


**Fig. 2:** Isothermal stress-controlled creep test

Isothermal experiments reveal that Haynes 230 was a complex material with varying behavior across the temperature spectrum. For the lower temperature ranges of 24 to 204°C (75 to 400°F) there was initial cyclic hardening followed by cyclic softening. In the intermediate temperature ranges of 427 to 760°C (800 to 1400°F) there was cyclic hardening without any stabilization. At high temperatures, i.e. greater or equal to 871°C (1600°F), there was either very little hardening or softening followed by saturation. Experiments with varying strain rates revealed that the material was rate-independent at temperatures equal to and lower than 760°C (1400°F). For temperatures equal to and greater than 871°C (1600°F) the material was rate-dependent. An experiment with strain holds (dwell periods) produce stress relaxation at temperatures in the rate-dependent regime, i.e. temperatures greater than or equal to 871°C (1600°F). However, at the lower temperatures of 649 and 760°C (1200 and 1400°F), though the material was mostly rate-independent with respect to different loading rates, there was still considerable stress relaxation.

Haynes 230 showed considerable creep across all temperatures investigated. Creep deformation is generally defined in three distinct stages: primary (transient), secondary (steady-state), and tertiary (accelerating) creep. The amount of each creep stage was a function of the temperature and the applied creep stress level. Haynes 230 showed that increasing the applied stress level at an elevated isothermal temperature results in increasing rates of creep accumulation that leads to failure.

## CONSTITUTIVE MODEL

A constitutive model is under development to simulate the wide range of experimental phenomena observed. A Chaboche type [6-8] modified viscoplastic constitutive model has been adopted. The decomposition of total strain ($\boldsymbol{\varepsilon}$) into elastic ($\boldsymbol{\varepsilon}^e$) and inelastic ($\boldsymbol{\varepsilon}^{in}$) portions follows the additive strain decomposition rule,

$$\boldsymbol{\varepsilon} = \boldsymbol{\varepsilon}^e + \boldsymbol{\varepsilon}^{in} \quad (1)$$

The elastic part obeys Hooke's law,

$$\boldsymbol{\varepsilon}^e = \frac{1+\nu}{E}\boldsymbol{\sigma} - \frac{\nu}{E}(tr\boldsymbol{\sigma})\mathbf{I} \qquad (2)$$

where $E$ and $\nu$ indicate Young's modulus and Poisson's ratio, respectively, $\boldsymbol{\sigma}$ and $\mathbf{I}$ are the stress and identity tensors, respectively, and *tr* is the trace operator.
The yield surface is represented by the von-Mises yield criterion as,

$$f(\boldsymbol{\sigma}-\boldsymbol{\alpha}) = \sqrt{\frac{3}{2}(\mathbf{s}-\mathbf{a}):(\mathbf{s}-\mathbf{a})} - \sigma_o = 0 \qquad (3)$$

Where, $\mathbf{a}$ is the back stress tensor, $\mathbf{s}$ and $\mathbf{a}$ are tensors of the deviators of the stress and back stress, respectively, and $\sigma_o$ is the yield stress.

A unified viscoplastic model has been chosen as it allows the modeling of rate-dependent behavior, an important feature particularly at higher temperatures. The inelastic strain rate is expressed as,

$$\dot{\boldsymbol{\varepsilon}}^{in} = \frac{3}{2}\dot{p}\frac{\mathbf{s}-\mathbf{a}}{J(\boldsymbol{\sigma}-\boldsymbol{\alpha})} \qquad (4)$$

where $(\dot{\bullet})$ denotes the differentiation with respect to time. $J(\boldsymbol{\sigma}-\boldsymbol{\alpha})$ is the second invariant norm, which is a scalar expressed as shown in (5).

$$J(\boldsymbol{\sigma}-\boldsymbol{\alpha}) = \left[\frac{3}{2}(\mathbf{s}-\mathbf{a}):(\mathbf{s}-\mathbf{a})\right]^{\frac{1}{2}} \qquad (5)$$

The plastic strain rate norm determines the type of flow rule one adopts, considering associative viscoplasticity for normality of viscoplastic flow. Three plastic strain rate norms are presented in the classical Norton's rule for secondary creep, Eq. (6), sine hyperbolic form of the Norton's rule, Eq. (7), and the product logarithm form of the Norton's rule, Eq. (8). $K$ and $n$ are rate-dependent parameters with a saturation parameter A and $\alpha$ for the sine hyperbolic and exponential form respectively. Each flow rule differs in the algebraic form of the viscoplastic strain rate norm as a function of the Norton's power law rule. All three forms are based on the Norton power law, which relates the secondary creep rate to the applied stress. As a result, the overstress, or distance from the current stress state to the yield surface is analogous to the stress applied in creep. Furthermore, the total inelastic strain rate in the unified model is analogous to the creep strain rate (see Eq. (4) and Eqs. (6-8)).

$$\dot{p} = \left\langle \frac{J(\boldsymbol{\sigma}-\boldsymbol{\alpha})-\sigma_o}{K} \right\rangle^n \qquad (6)$$

$$\dot{p} = A\sinh\left( \left\langle \frac{J(\boldsymbol{\sigma}-\boldsymbol{\alpha})-\sigma_o}{K} \right\rangle^n \right) \qquad (7)$$

$$\dot{p} = \left\langle \frac{J(\boldsymbol{\sigma}-\boldsymbol{\alpha})-\sigma_o}{K} \right\rangle^n e^{\alpha\left\langle \frac{J(\boldsymbol{\sigma}-\boldsymbol{\alpha})-\sigma_o}{K} \right\rangle^n} \qquad (8)$$

A Chaboche nonlinear kinematic hardening rule with four superimposed back stresses is chosen (Eq. (9)). The kinematic hardening rule describes the evolution of the back stress and has the features of dynamic recovery, and static recovery. The static recovery term is essential for the simulation of rate-dependent behavior such as stress relaxation and creep. Simulations of the stress relaxation behavior at half-life under dwell condition, is one of the most important deformation behaviors in terms of creep-fatigue damage analysis of the actual components [11].

$$\mathbf{a} = \sum_{i=1}^{4}\mathbf{a}_i$$
$$\dot{\mathbf{a}}_i = \frac{2}{3}C_i\dot{\boldsymbol{\varepsilon}}^{in} - \gamma_i\mathbf{a}_i\dot{p} - b_i J(\mathbf{a}_i)^{r-1}\mathbf{a}_i \qquad (9)$$
$$\text{i} = 1 \text{ to } 4$$

*Strain range dependence*

The effect of strain range on the shape of the hysteresis loops has been shown to vary dramatically [8-9]. The importance of capturing the shape of the hysteresis loops as closely as possible has been shown [9] to have an impact in the overall simulation quality. While the preceding equations are able to model each strain range well independently, they require different model parameters for each strain range. As a result, it is important to develop a modeling scheme that is capable of simulating all strain range hysteresis responses. To overcome this challenge, strain range dependence is modeled by considering a strain memory surface which memorizes the prior largest plastic strain range [8-9, 13]. The radius and center of the strain memory surface are $q$ and $\mathbf{Y}$ respectively. The memory surface equation is given by Eq. (10) and the evolution equations of $q$ and $\mathbf{Y}$ are given by Eq. (11) and Eq. (12), respectively. Material constant $\eta$ can be determined from uniaxial response and are related to the stabilized plastic strain amplitudes. Here, $\eta$ governs the isotropic expansion of the surface in Eq. (11) and (1-$\eta$) governs the kinematic movement of the surface in Eq. (12). $H(g)$ is the Heaviside step function. The kinematic hardening dynamic recovery parameters $\gamma_i$ of Eq. (9) are varied with

cycles and are functions of $q$. The evolutions of $\gamma_i$ occur according to Eq. (14) to Eq. (15).

$$g = \left[\frac{2}{3}\left(\boldsymbol{\varepsilon}^{in} - \mathbf{Y}\right) : \left(\boldsymbol{\varepsilon}^{in} - \mathbf{Y}\right)\right]^{\frac{1}{2}} - q = 0 \qquad (10)$$

$$\dot{q} = \left[\eta H\left(g\right)\left\langle \mathbf{n} : \mathbf{n}^{*}\right\rangle\right]\dot{p} \qquad (11)$$

$$\dot{\mathbf{Y}} = \sqrt{3/2}\left[\left(1-\eta\right)H\left(g\right)\left\langle \mathbf{n} : \mathbf{n}^{*}\right\rangle \mathbf{n}^{*}\right]\dot{p} \qquad (12)$$

$$\mathbf{n}^{*} = \sqrt{\frac{2}{3}}\frac{\boldsymbol{\varepsilon}^{in} - \mathbf{Y}}{q} \qquad (13)$$

$$\dot{\gamma}_i = D_{\gamma i}\left(\gamma_i^{AS}\left(q\right) - \gamma_i\right)\dot{p} \qquad (14)$$

$$\gamma_i^{AS}\left(q\right) = a_{\gamma i} + b_{\gamma i}e^{-c_{\gamma i}q} \qquad (15)$$

*Mean stress evolution*

The cyclic evolution of Haynes 230 for fatigue-creep experiments (strain-dwells) shows non-zero mean stresses that evolve with cycles when compared to tests without strain dwells. In addition, for thermo-mechanical fatigue (TMF) responses significant mean stress is developed for both in-phase (IP) and out-of-phase (OP). In our modeling scheme this mean stress evolution must be accounted whether it is isothermal or anisothermal. It has been shown by Yaguchi et al. [11] that the evolution of mean stresses can be simulated by modifying the non-linear kinematic hardening rule (Eq. 9) as Eq. (16) through incorporating a tensor $\mathbf{Y_{bi}}$ in the dynamic recovery term (the second term).

$$\begin{aligned} \mathbf{a} &= \sum_{i=1}^{4}\mathbf{a}_i \\ \dot{\mathbf{a}}_i &= \frac{2}{3}C_i\dot{\boldsymbol{\varepsilon}}^{in} - \gamma_i\left(\mathbf{a}_i - \mathbf{Y}_{\mathbf{b}i}\right)\dot{p} - b_i J\left(\mathbf{a}_i\right)^{r-1}\mathbf{a}_i \end{aligned} \qquad (16)$$

This form of the dynamic recovery was first introduced by Chaboche-Nouailhas [14] however its behavior and evolution is different in the Yaguchi model. The driving force of $\mathbf{Y}_{\mathbf{b}i}$ as in Eq. (17) is assumed to be rate/time-dependent deformation as the dislocation networks generally form under creep conditions,

$$\dot{\mathbf{Y}}_{\mathbf{b}i} = -\alpha_{b,i}\left\{Y_{st,i}\frac{\mathbf{a}_i}{J\left(\mathbf{a}_i\right)} + \mathbf{Y}_{\mathbf{b}i}\right\}\left\{J\left(\mathbf{a}_i\right)\right\}^{r_i} \qquad (17)$$

Ahmed et al. [12] demonstrated the implementation of Eqs (16) and (17) into the four-term Chaboche nonlinear kinematic hardening rule [6-8] for effective simulation of thermo-mechanical fatigue-creep responses. The same model development is implemented here for simulating mean stress evolution of the isothermal fatigue and fatigue-creep responses.

## PARAMETER DETERMINATION

The simulation of the experimental responses using the modified viscoplastic constitutive model needs determination of a number of material parameters. The material parameters are associated with all the modeling features presented herein which include: rate-independent kinematic parameters, strain-range dependent parameters, rate-dependent parameters, static recovery parameters, and mean stress evolution parameters. The steps for the parameter determination for the modified viscoplastic constitutive model are following:

1. Strain-controlled uniaxial isothermal experiments without any peak strain hold are used to determine the rate-independent kinematic hardening parameters. An automated genetic algorithm-based optimization scheme was adopted for determining these parameters.
2. Experiments at different loading rates (with no hold times) are used for rate-dependent parameter determination. The viscosity function includes the Norton rate dependent parameters $K$ and $n$ along with any saturation parameters depending on the viscosity form. For Haynes 230, the rate dependent parameters were only needed for temperatures above 760°C, while for temperatures below this the material was assumed to behave rate-independent, which behavior was obtained as a limiting case of viscoplasticity.
3. For strain range dependence, the parameter determination followed the same temperature bounds as the rate-dependent parameters, where for temperatures below 760°C strain range dependent parameters were needed, while above this temperature strain range dependent parameters were made the limiting case as if one strain range was used in the parameter determination.
4. In the above steps, static recovery parameters were neglected. However, once the above steps were completed, the isothermal strain controlled experiments with strain hold times are used to determine the static recovery parameters of kinematic hardening. As genetic-algorithm coding is not completed yet for all model parameter determination, a nonlinear gradient-based optimization procedure is used to optimize the stress relaxation responses with cycles.
5. Finally, from the thermo-mechanical responses the mean stress parameters are finalized for optimizing the mean stress with cycles using a nonlinear gradient-based optimization procedure.

## SIMULATIONS

The capability of the modified viscoplastic model in simulating a wide range of material responses was evaluated against the broad set of isothermal uniaxial experiments with

multiple strain ranges, strain rates, and fatigue-creep (strain-dwell) across a broad temperature range (24-982°C). For each temperature level, only one set of parameters was determined. The performance of the model in predicting the experimental responses was evaluated based on the stress-strain hysteresis loop shape, stress amplitude and mean, along with fatigue-creep stress relaxation during a strain dwell. In addition, the performance of the model was evaluated for not only strain-controlled loading histories as shown in Figs. 1a-b, but also the capability of the model in simulating stress-controlled responses for creep loading shown in Fig. 2. In the literature, the simulation of fatigue-type loading with some creep damage given by fatigue-creep strain dwells, along with pure creep-type loading is rarely done. Few studies have attempted to model both fatigue and creep [15-16]. However, in both of these studies the simulations of the full creep responses were not shown.

*Effect of Strain Range Dependence for Isothermal LCF*

The importance of capturing the shape of the hysteresis loops as closely as possible has been shown to have an impact in the overall simulation quality [9]. For a better prediction of the material response, it is essential to simulate the hysteresis loop shape accurately, in addition to the cyclic hardening/softening behavior. The cyclic response of Haynes 230 was dependent on strain range and this behavior was achieved through the evolution of kinematic hardening parameters. Strain range dependence was modeled by considering a strain memory surface which memorizes the prior largest plastic strain range. The kinematic hardening parameters $\gamma_i$ are varied with cycles and are functions of the size of the strain memory surface. This strain memory surface size stabilizes to half the width of the largest hysteresis loop in the history of loading. The modeling capability of strain range dependence allows one to specify, for a particular temperature, an evolution equation for the Chaboche parameters as a function of the strain range which is physically linked to the hysteresis responses. Kinematic hardening of Haynes 230 was only needed as it was observed that the yield surface size stayed almost the same for a particular temperature. The performance of the model for strain range dependence is shown in Figs. 3-4. Figure 3 shows the capability of the model to simulate the hysteresis loop shape along with the peak stresses for a particular strain range. Figure 4 shows for various strain ranges the simulation of the model for the peak stresses. The chosen temperature for discussion was 427°C (800°F) where the material shows continuous cyclic hardening without stabilization. For all temperatures less than 760°C (1400°F) strain range dependence modeling was used which were also considered to be rate-independent temperatures from experimental responses.

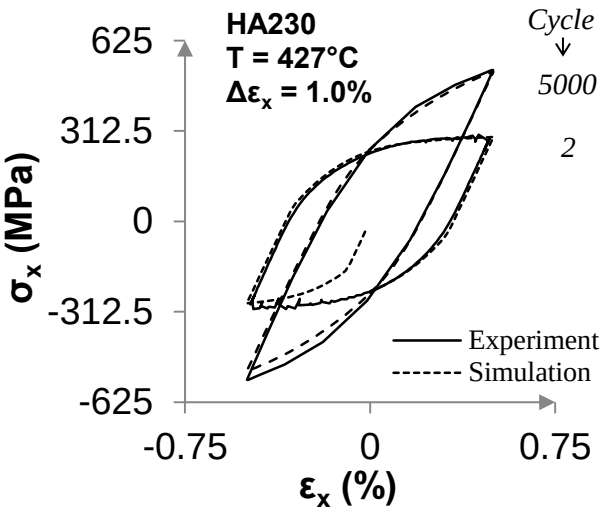


**Fig. 3:** Simulation of hysteresis loops at 427°F for initial and half-life cycles

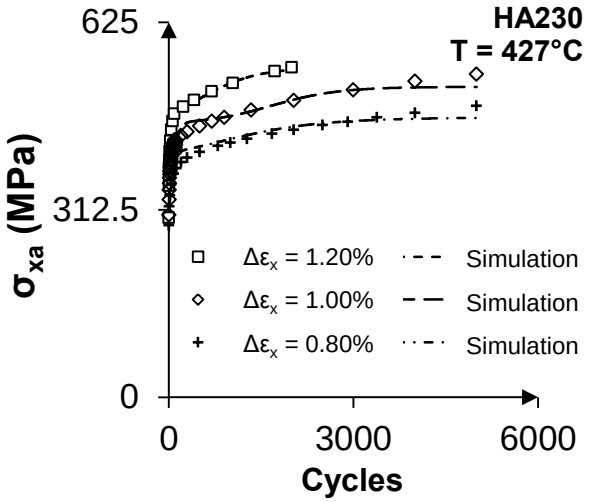


**Fig. 4:** Simulation of stress amplitudes with cycles at 427°C for different loading strain ranges

*Rate-dependence Simulations*

The plastic strain rate norm (Eq. 4) determines the type of flow rule one can adopt in simulating the rate-dependent behavior of a material. The relation between this viscous stress and the plastic strain rate norm is usually highly nonlinear. In our study, we explored the Norton's power law (Eq. 6), the sine hyperbolic form of the Norton's power law (Eq. 7), and the exponential form of the Norton's power law (Eq. 8). The simulation capability of classical Norton's and the sine hyperbolic has shown to produce similar results even the extra saturation parameter A in Eq. 7. Both flow rules perform extremely well when rate saturation is not an issue, which was the case at 982°C (1800°F). However, at temperatures 816°C (1500°F) and 871°C (1600°F) Haynes 230 showed a degree of

saturation when comparing the 2 cpm and 20 cpm experimental responses. As a result, the exponential Norton of Eq. (8) was implemented and shown to perform better with respect to the rate saturation. The simulations of the modified Chaboche model are presented in Figs. 5-6 for the exponential Norton's flow rule Eq. (8) to show the strength of the model with rate saturation and various strain rates. Figure 5a-b shows that through the rate-dependent parameters we can simulate hysteresis loops from different strain rates. Figure 6 shows directly the positive strain rate dependent behavior of Haynes 230 with the rate saturation going from 2 cpm to 20 cpm as the stress amplitudes begin to saturate. Similar simulations are obtained for rate-dependent temperatures (>760°C).

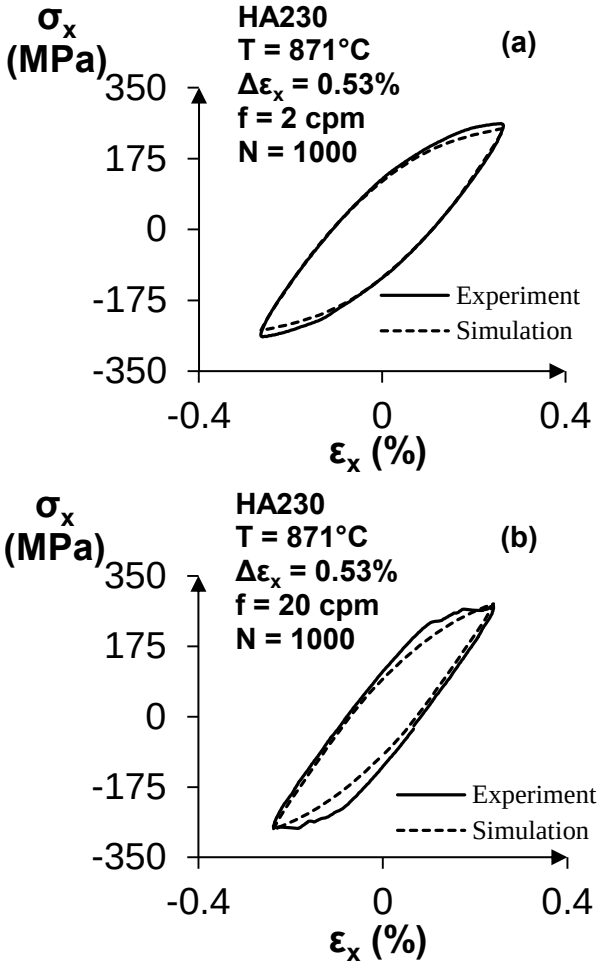


**Fig. 5:** Simulation of hysteresis loops at 871°C for different strain rates: (a) 2 cpm, and (b) 20 cpm

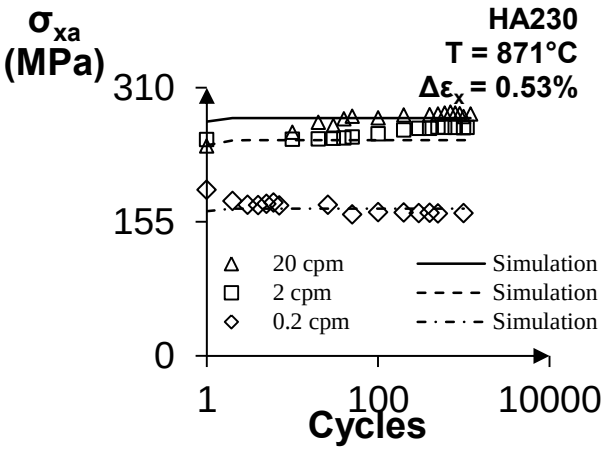


**Fig. 6:** Simulation of stress amplitudes with cycles at 871°C for different strain rate

*Fatigue-Creep (Strain-Dwell) Simulations*

The modeling of stress relaxation has been performed for isothermal cyclic strain controlled experiments with strain holds at the peak compressive strain. The accurate modeling of stress relaxation is very important to reliably predict creep-fatigue interaction. Haynes 230 was overall rate-independent ($\leq$ 760°C) but still shows stress relaxation for strain holds for this temperature range. The stress relaxation has been modeled through the static recovery term in the Chaboche kinematic hardening rule (Eq. (16)). For higher temperatures ($\geq$ 871°C) the simulation of stress relaxation used both the rate-dependence of the flow rule (Eq. 4) and static recovery (Eq. 16). The simulation of the stabilized hysteresis loop ($600^{th}$ cycle) for 60s hold at 982°C (1800°F) is shown in Fig. 7. In addition, the ability of the model to simulate the stress relaxation of the material with cycles for creep temperatures are shown in Fig. 8 for 60s hold (strain-dwell) tests. In Fig. 8, normalized stress relaxation is shown, which was computed by taking the stress relaxation (stress difference before and after the strain hold) and dividing it by the compressive peak of each cycle.

*Creep Simulation*

The modeling of both fatigue and creep is a major challenge with the constitutive models available in the literature. Currently, the modified Chaboche model used to simulate the fatigue and fatigue-creep responses of Haynes 230 performs well for not only isothermal, but also anisothermal thermo-mechanical fatigue [14]. However, the simulation of creep responses showed that the model over predicts the creep responses for all temperatures. In Fig. 9, one such temperature is shown whereby the model tends to over predict the creep response of the material. However, at this same temperature 871°C in Fig. 8 one can see that the stress relaxation responses of the fatigue-creep test (strain-dwells) perform well. It can be shown that the creep response is highly dependent on the static recovery parameters of the model in

Eq. (16) of the kinematic hardening rule. The challenge will be in finding one parameter set at each temperature with static recovery that is capable of simulating both the fatigue response (strain-controlled) and creep response (stress-controlled), and there by creep-fatigue response.

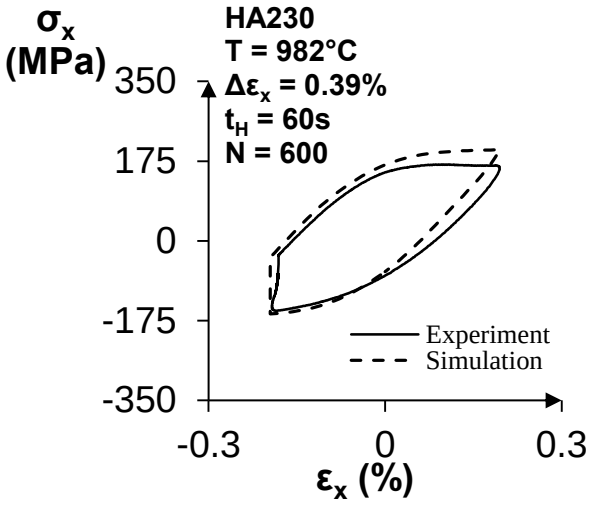


**Fig. 7:** Simulation of hysteresis loops at 871°C for different strain rates: (a) 2 cpm, and (b) 20 cpm

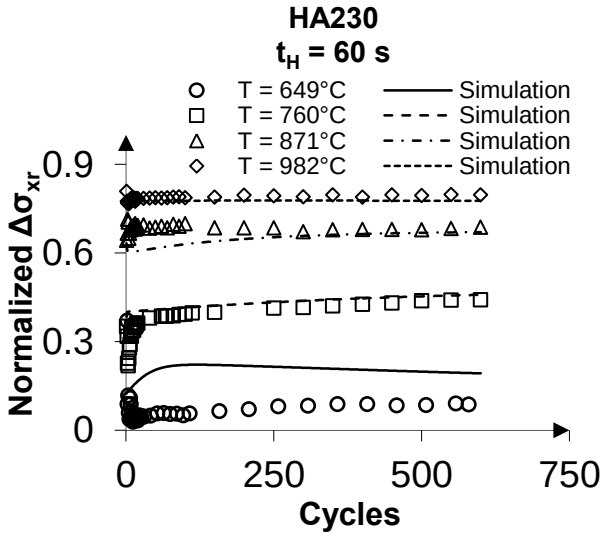


**Fig. 8:** Simulation of hysteresis loops at 871°C for different strain rates: (a) 2 cpm, and (b) 20 cpm

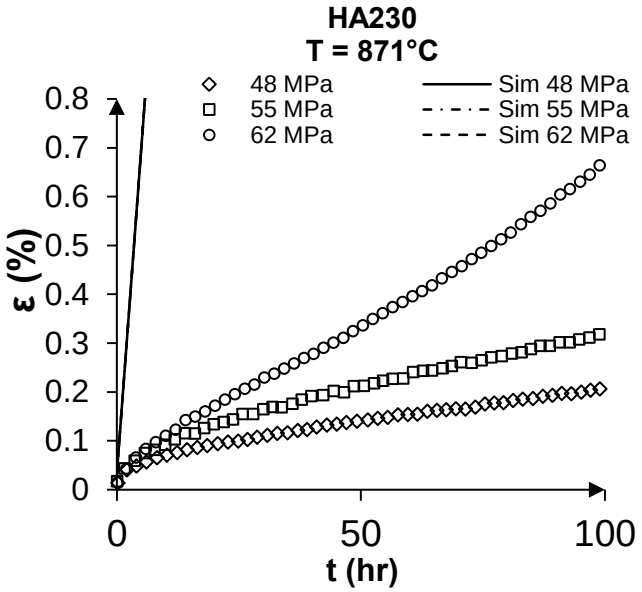


**Fig. 8:** Simulation of creep at 871°C for different applied creep stresses

## CONCLUSIONS

Haynes 230 is a complex material showing a wide range of material responses. In design-by-analysis of components it is important to simulate the material behavior as accurately as possible, which requires a robust constitutive model. A modified Chaboche model was shown for unified viscoplasticity with several added features including: strain-range dependence, strain-rate dependence, static recovery, and mean-stress evolution. The simulations of the model perform well for both low-cycle fatigue and fatigue-creep. However, creep responses of Haynes 230 were over predicted. Further investigation is needed in order to overcome the deficiencies of the model in simulating both fatigue and creep.

## ACKNOWLEDGEMENTS

The authors are grateful to Honeywell Aerospace for the financial support of the project. Discussions with Dr. Menon in developing and performing the project tasks were invaluable. Experiments were conducted by Element in Cincinnati, Ohio.

## REFERENCES

[1] Hasselqvist, M., (2002). Viscoplastic modeling for Industrial Gas Turbine (IGT) application with emphasis on the sheet material Haynes 230. *Proc. ASME Turbo Expo, GT2002-30659*.

[2] Hasselqvist, M., (2004). TMF crack initiation lifing of austenitic carbide precipitation alloys. *Proc. ASME Turbo Expo, Vienna, GT2004-54333*.

[3] Mannan, S.L. and Valsan, M., (2006). High-temperature low cycle fatigue, creep-fatigue and thermomechanical fatigue of steels and their welds. *Int. J. of Mech. Sci, 48*(2), 160-175.

[4] Nagesha, A., Kannan, R., Sastry, G.V.S., Sandhya, R., Singh, V., Rao, K.B.S. and Mathew, M.D. (2012). Isothermal and thermomechanical fatigue studies on a modified 9Cr-1Mo ferritic martensitic steel. *Mat. Sci. Eng. A, 554*, 95-104.

[5] Rao, K., Meurer, H., Schuster, H., 1988. Creep-fatigue interaction of inconel 617 at 950°C in simulated nuclear reactor helium. Materials Science and Engineering: A, 104 pp. 37-51.

[6] Chaboche, J. L., (1986). Time-Independent Constitutive Theories for Cyclic Plasticity. International Journal of Plasticity, 2(2), 49-188.

[7] Chaboche, J. L., (1989). Constitutive Equations for Cyclic Plasticity and Cyclic Viscoplasticity. International Journal of Plasticity, 5(3) 247-302.

[8] Chaboche, J.L., (2008). A review of some plasticity and viscoplasticity constitutive theories. Int. J. Plasticity 24, 1642–1693.

[9] Krishna, S., Hassan, T., Ben Naceur, I., Saï, K., Cailletaud, G., (2009). Macro versus micro-scale constitutive models in simulating proportional and nonproportional cyclic and ratcheting responses of stainless steel 304. Int. J. Plast. 25, 1910–1949.

[10] Chaboche, J. L., Dang Van, K. and Cordier, G., (1979). Modelization of the strain memory effect on the cyclic hardening of 316 stainless steel. ONERA, TP no. 1979-109, L 11/3.

[11] Yaguchi, M., Yamamoto, M., and Ogata, T., (2002). A viscoplastic constitutive model for nickel-Base superalloy, part 1: kinematic hardening rule of anisotropic dynamic recovery. International Journal of Plasticity, 18(8) 1083-1109.

[12] Ahmed, R., Barrett, P.R., Hassan, T., 2013, "Constitutive Modeling of Haynes 230 for Anisothermal Thermo-mechanical fatigue and multiaxial creep-ratcheting responses" 2013 ASME Pressure Vessels & Piping Conference (Paper No. PVP2013-97248), July 14-18, 2013, Paris, France.

[13] Nouailhas, D., Cailletaud, G., Policella, H., 1985, "On the Description of Cyclic Hardening and Initial Cold Working," Engineering Fracture Mechanics, 21(4) pp. 887-895.

[14] Chaboche, J.L., Nouailhas, D., 1989, "Constitutive modeling of ratcheting effects – part 2: possibilities of some additional kinematic rules," ASME J. Eng. Mat. Tech. 111, pp. 409-416

[15] Barrett, R. A., O'Donoghue, P. E., & Leen, S. B. (2012). An improved unified viscoplastic constitutive model for strain-rate sensitivity in high temperature fatigue. International Journal of Fatigue, 48, 192-204.

[16] Kuna, M., & Wippler, S. (2010). A cyclic viscoplastic and creep damage model for lead free solder alloys. Engineering Fracture Mechanics, 77(18), 3635-3647.